Supporting Information

Atomic-scale insight into the enhanced surface stability of methylammonium lead iodide perovskite by controlled deposition of lead chloride

Afshan Jamshaid [†,a], Zhendong Guo [†,b], Jeremy Hieulle [a], Collin Stecker [a], Robin Ohmann [a,‡], Luis K. Ono [a], Longbin Qiu [a], Guoqing Tong [a], Wanjian Yin [*,b], Yabing Qi [*,a]

[a] *Energy Materials and Surface Sciences Unit (EMSSU), Okinawa Institute of Science and Technology Graduate University (OIST), 1919-1 Tancha, Onna-son, Okinawa 904-0495, Japan.*

[b] *College of Energy, Soochow Institute for Energy and Materials Innovations (SIEMIS) and Jiangsu Provincial Key Laboratory for Advanced Carbon Materials and Wearable Energy Technologies, Soochow University, Suzhou 215006, China.*

[†] *These authors contributed equally to this work.*

[*] Corresponding authors: Yabing Qi, Yabing.Qi@OIST.jp; Wanjian Yin, wjyin@suda.edu.cn.

[‡] *Current address: Department Physik, Universität Siegen, 57068 Siegen, Germany.*

KEYWORDS: $MAPbI_3$, STM, DFT, Cl incorporation, XPS/UPS/IPES

Table of contents:

Supplementary Section 1. Perovskite surface bandgap combined with the analyses of energy level alignments in a solar cell device

Supplementary Figs (Figs S1-S8)

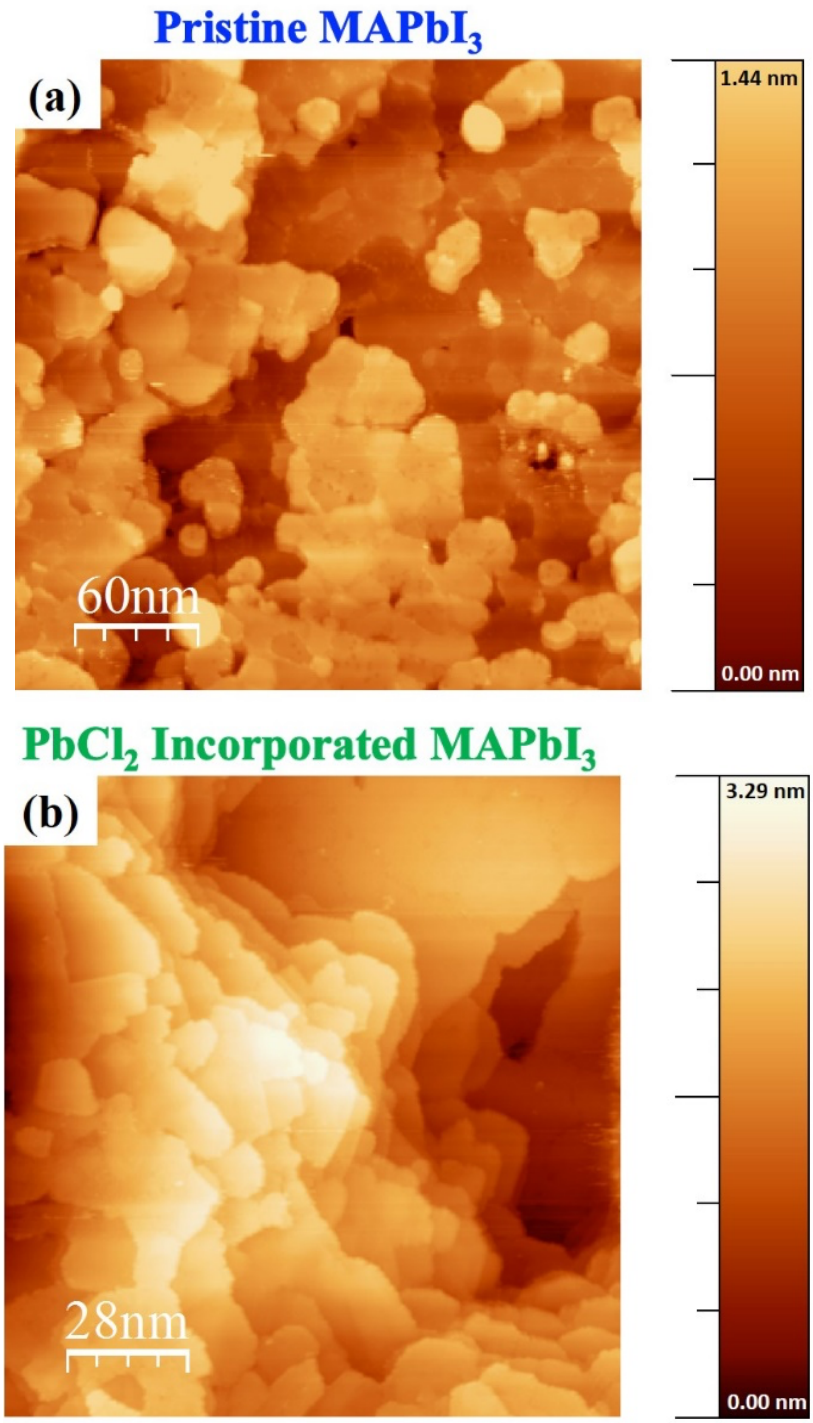

Fig S1: (a) Large area STM image of pristine $MAPbI_3$ showing the typical grains (Scan area = 300 × 300 nm^2; Sample bias voltage = –2.5 V; Tunnelling current = 50 pA). (b) Large area STM image of Cl incorporated $MAPbI_3$ showing the typical grains (Scan area = 300 × 300 nm^2; Sample bias voltage = –2.5 V; Tunnelling current = 70 pA).

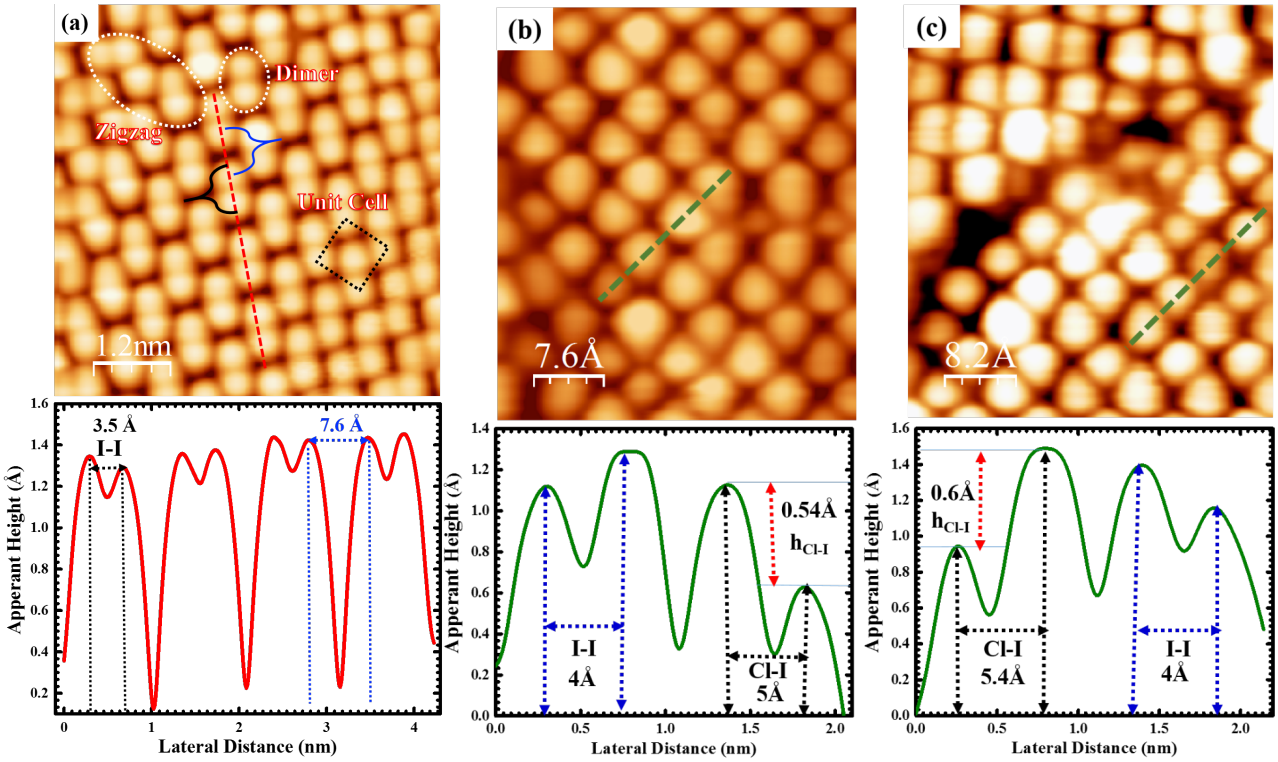

Fig S2. LT-STM images of the pristine and Cl incorporated $MAPbI_3$ perovskite thin films deposited on Au (111). (a) High resolution image of iodine dimer (labeled by white dashed ellipse) and iodine zigzag (labeled by white dashed ellipse and black dashed rectangle) structure (Scan area = 4.0 × 4.5 nm^2, Sample bias voltage = –2.70 V; Tunneling current = 10 pA). Height profiles of the observed domain labeled by red broken lines. (b) LT-STM image of 0.5 ML of $PbCl_2$ (4 min of deposition) incorporation in the center of a grain of the $CH_3NH_3PbI_3$ perovskite. Height profiles of observed Cl incorporation in the dimer structures labeled by a black dashed circle (Scan area = 3.7 × 4.8 nm^2, Sample bias voltage = –2.50V; Tunneling current = 100 pA). (c) Incorporated Cl close to the grain boundary labeled by the black dashed rectangle. Height profile of the observed Cl depression close to the grain boundary labeled by a white dashed circle (Scan area = 4.6 × 5.3 nm^2, Sample bias voltage = –2.50V; Tunneling current = 100 pA).

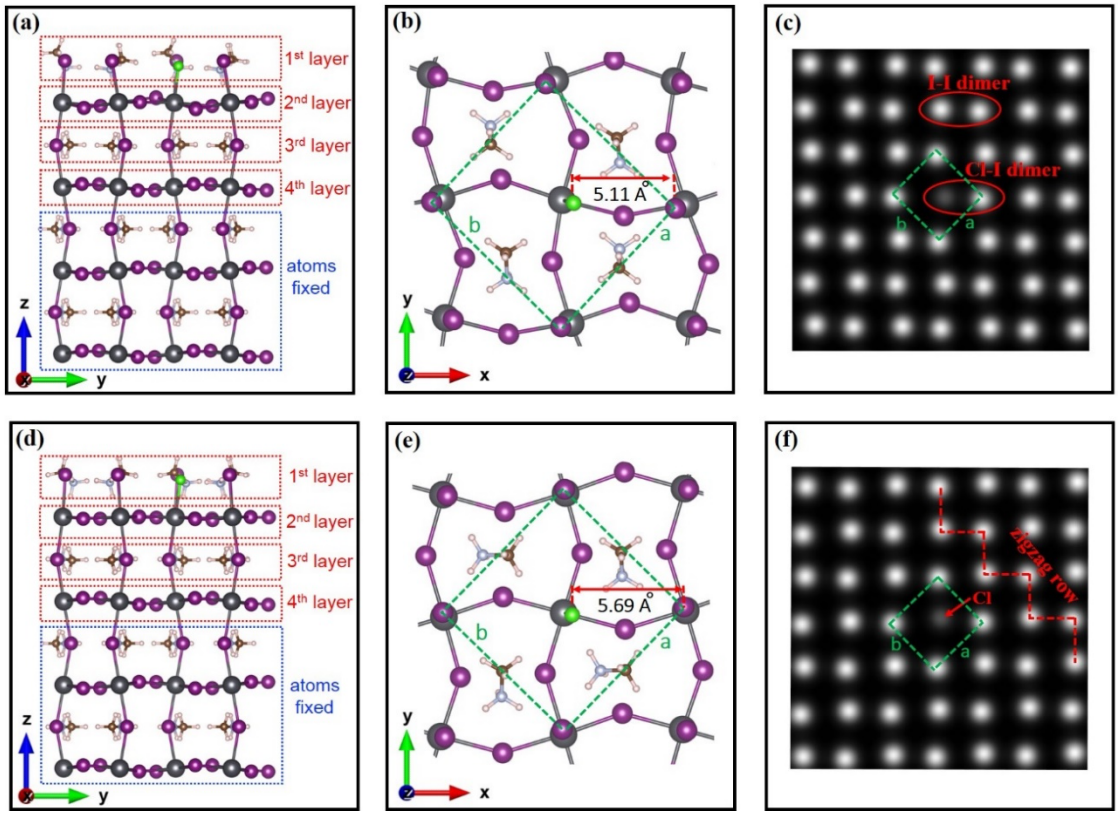

Fig S3: Geometrical dimer and zigzag structures of Cl incorporated $MAPbI_3$ (001) surfaces obtained by DFT calculations. (a) The side view, (b) top view of the Cl incorporated dimer structure and Cl-I bond length. (c) Simulated STM image. (d) The side view, (e) top view of the Cl incorporated zigzag structure and Cl-I bond length. (f) Simulated STM image.

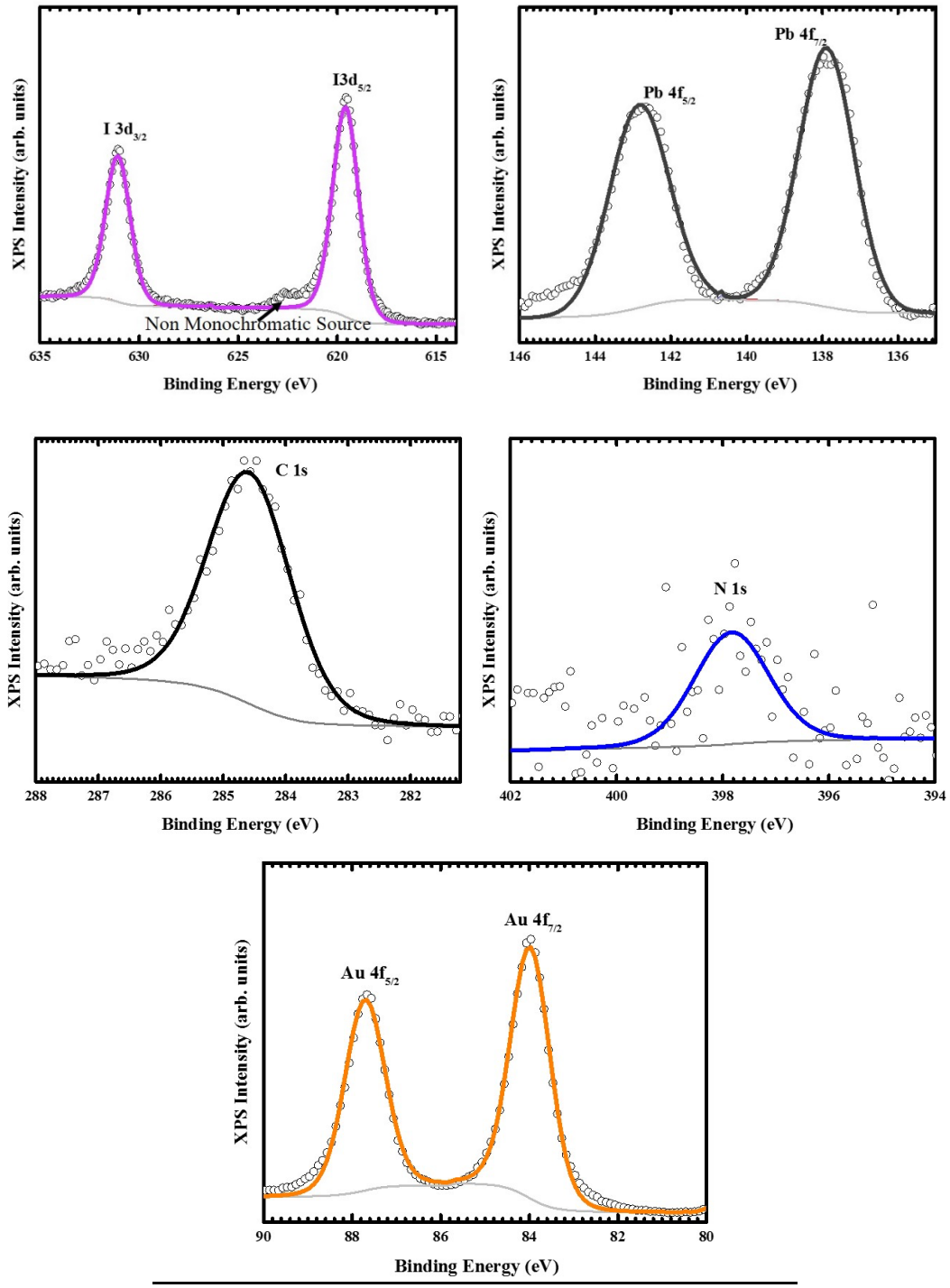

$MAPbI_3$ Deposition Time	Pb 4f, I 3d ratio	$MAPbI_3$
3 minutes	[Pb] : [I] = 1 : 3	$MAPbI_3$

Fig S4. XPS spectra and chemical composition determination of the pristine $MAPbI_3$ thin film. The non-monochromatic source related peak is indicated by an arrow in the I 3d core level region..

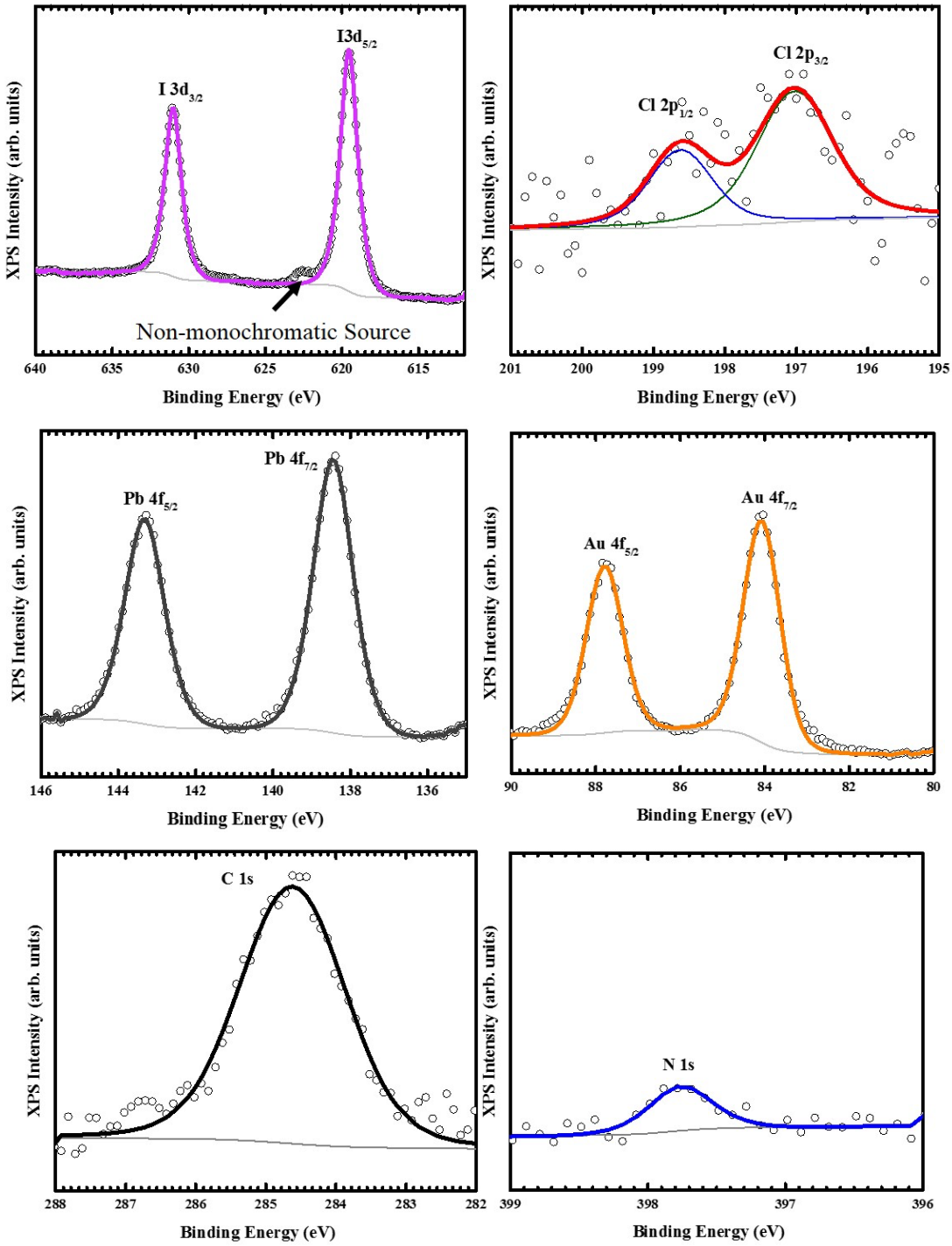

MAPbI$_3$ Deposition Time	Pb 4f, I 3d, Cl 2p ratio	MAPb(I$_{1-x}$Cl$_x$)$_3$
6 minutes	[Pb] : [I] : [Cl] =1 : 2.8 : 0.21	MAPbI$_{2.59}$Cl$_{0.21}$

Fig S5. XPS spectra and chemical composition determination of the MAPbI$_3$ thin film after 0.75 ML deposition of PbCl$_2$.

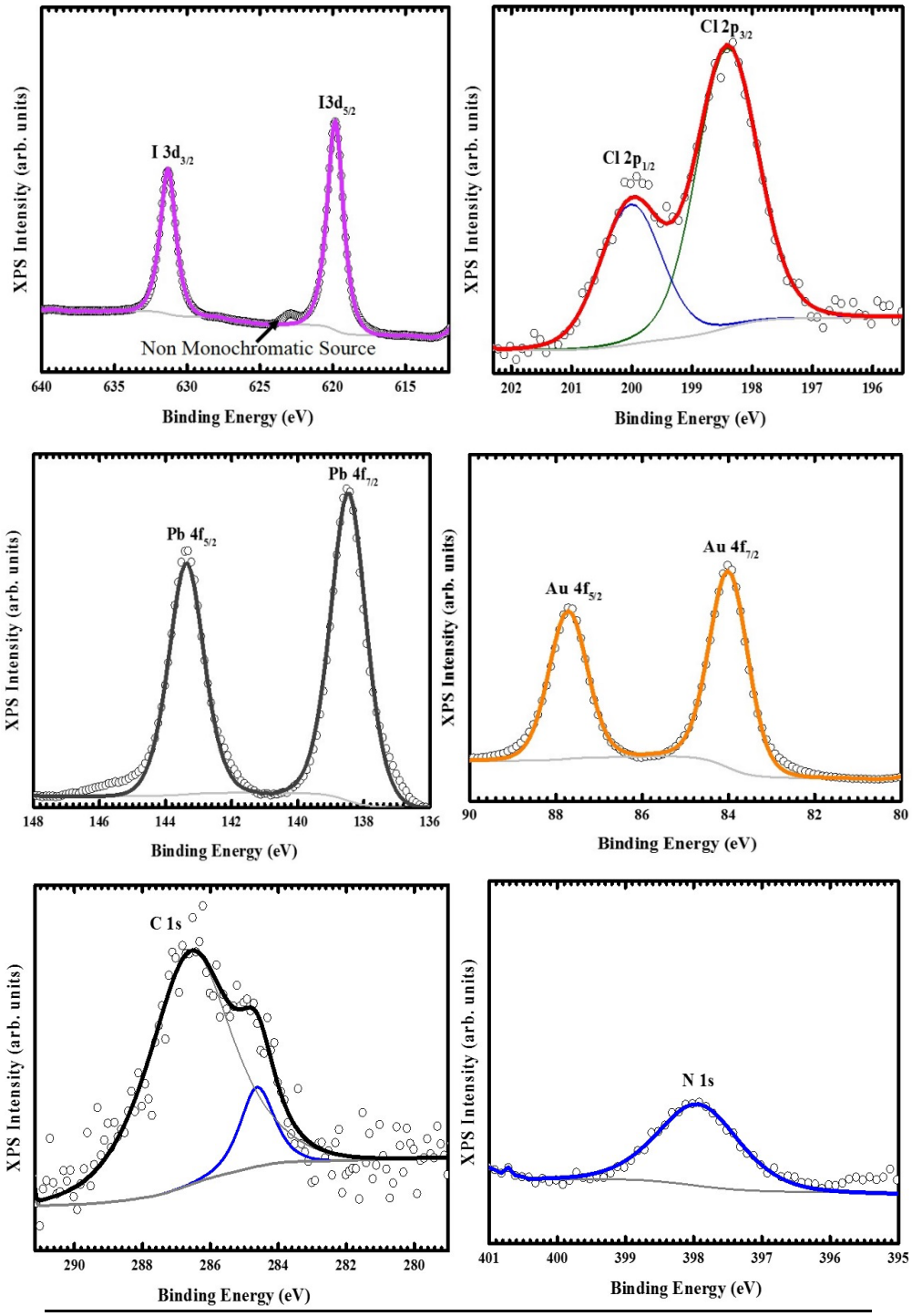

$MAPbI_3$	Pb 4f, I 3d, Cl 2p ratio	$MAPb(I_{1-x}Cl_x)_3$
Deposition Time		
12 minutes	[Pb] : [I] : [Cl] = 1 : 3.5 : 0.8	$MAPbI_{2.7}Cl_{0.8}$

Fig S6. XPS spectra and chemical composition determination of the $MAPbI_3$ thin film after 1.5 ML deposition of $PbCl_2$.

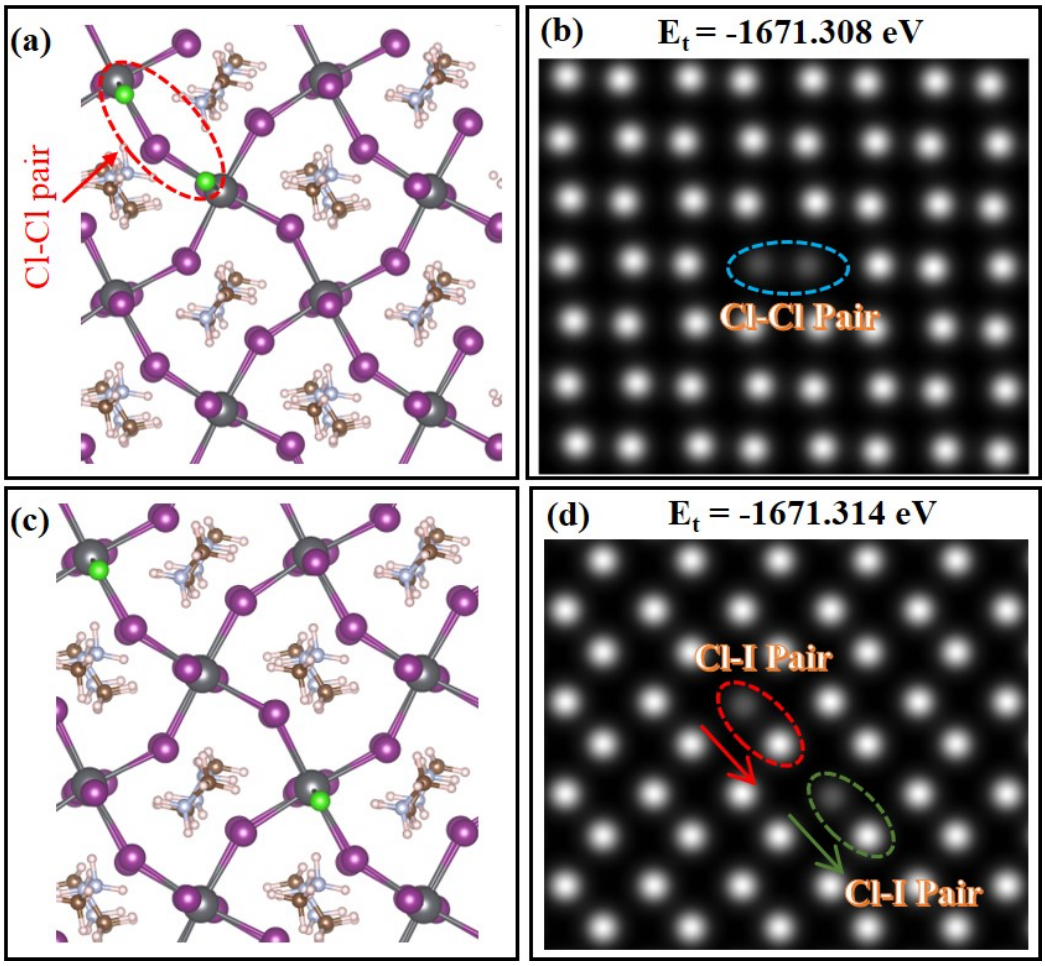

Fig S7: Possible configurations of (a,b) one Cl-Cl pair and (c,d) two Cl-I pairs appearing in the dimer structure predicted by DFT calculations. E_t = total energy.

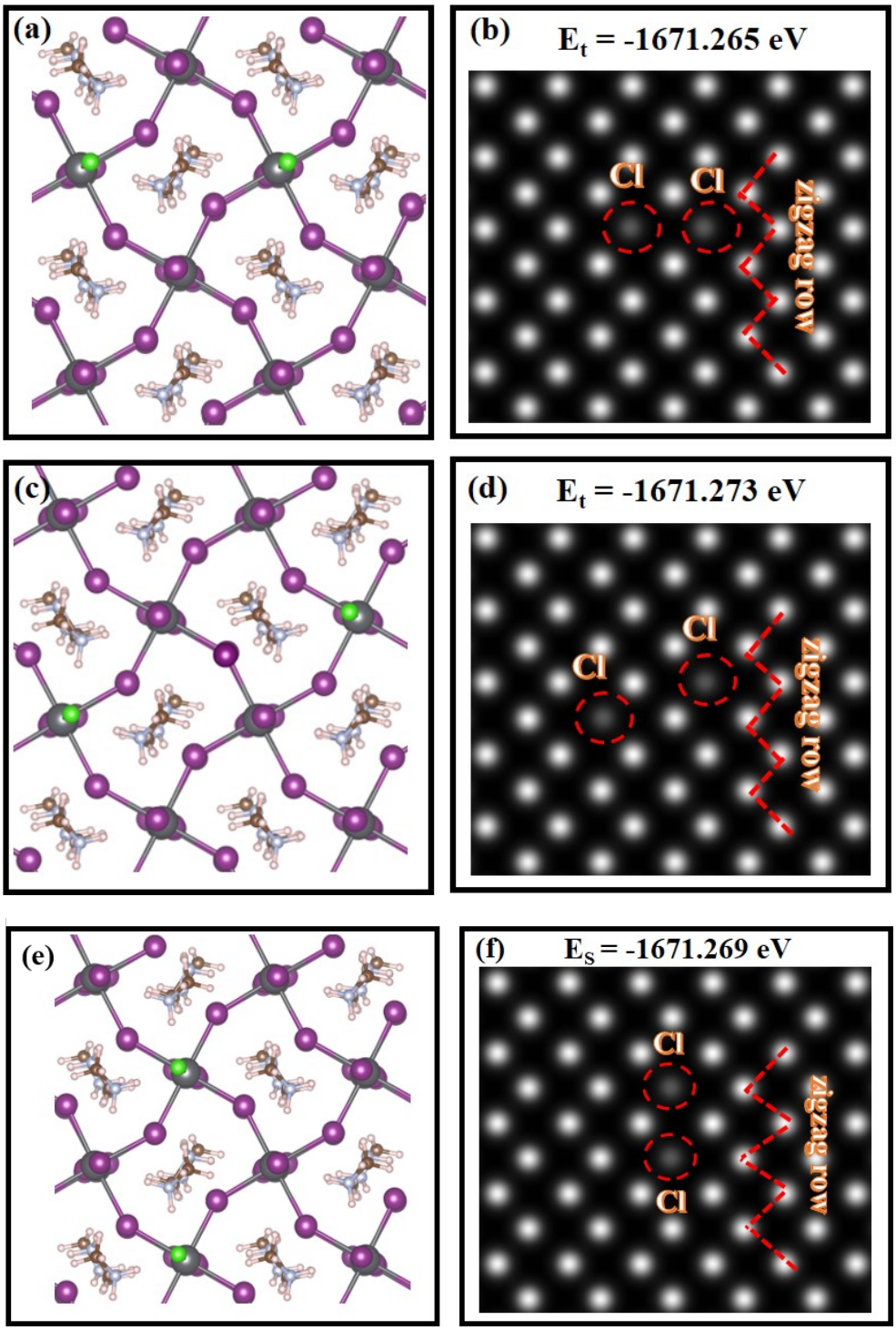

Fig S8: Possible configurations of two Cl-I pairs appearing in the zigzag structure predicted by DFT calculations. E_s = surface energy.

Supplementary Section 1. Perovskite surface bandgap combined with the analyses of energy level alignments in a perovskite solar cell device

To evaluate the effects of surface bandgap increase from 1.13 eV (pristine $MAPbI_3$) to 1.62 eV (Cl-incorporated $MAPbI_3$) on the device performance, the energy level alignments at the perovskite/ETL and perovskite/HTL interfaces were analysed (ETL = electron transport layer and HTL = hole transport layer). As an example for the analyses, we considered a well-established regular device structure composed of TiO_2 as ETL and 2,2',7,7'-Tetrakis[N,N-di(4-methoxyphenyl)amino]-9,9'-spirobifluorene (spiro-MeOTAD) as HTL [1 2 3]. The valence band maximum (VBM) values for the pristine $MAPbI_3$ and the Cl-incorporated $MAPbI_3$ were determined by UPS measurements (Figures S9(a) and S10(a-d)) and the conduction band minimum (CBM) values were determined by IPES measurements (Figures S9(b) and S10(e-h)). The energy diagrams considering pristine $MAPbI_3$ and Cl-incorporated $MAPbI_3$ sandwiched by ETL and HTL are illustrated in Figures S9(c,d), respectively. The VBM and CBM values were referenced with respect to (w.r.t.) the Fermi level (0 eV). The difference in the energy barrier between the CBM values of pristine $MAPbI_3$ and TiO_2 reduces from ~0.15 eV (Figure S9(c)) down to ~0.03 eV (Figure S9(d)) when Cl is incorporated on the $MAPbI_3$ surface, suggesting the enhancement in open-circuit voltage (Voc) of the device. Furthermore, because the Cl-incorporated $MAPbI_3$ still shows a small barrier for electron extraction (i.e., less driving force for electron extraction from the perovskite to TiO_2 ETL), the current density (Jsc) is expected to be not optimal [1]. A similar analysis is performed on the perovskite/HTL side. The energy difference between VBM of the pristine $MAPbI_3$ perovskite and the highest occupied molecular orbital (HOMO) of spiro-MeOTAD increases from ~0.11 eV (Figure S9(c)) to ~0.48 eV (Figure S9(c)) when Cl is incorporated on $MAPbI_3$ surface,

which leads to decrease in the overall Voc of the device. The driving force for the hole extraction is enhanced for the Cl-incorporated $MAPbI_3$, but further enhancement in Jsc of this device may not be expected as Jsc is limited by the small energy barrier differences at the perovskite/ETL interface. Therefore, in terms of Voc, Cl-incorporated $MAPbI_3$ surface would be beneficial at the interface formed with the TiO_2 ETL, but detrimental at the interface formed with the spiro-MeOTAD HTL. Cl-incorporated perovskites are also advantageous in tandem solar cells. For single-junction cells, the bandgap from 1.3 eV to 1.4 eV is ideal [5]. But for two-junction tandem solar cells, the larger bandgap is desirable [6]. Thus, bandgap tuning by Cl incorporation in the $MAPbI_3$ can make it a better choice as the top cell in a tandem solar cell. However, it is important to note that in this study, Cl incorporation mainly occurs at the surface and thus such a bandgap increase effect is only valid for the surface.

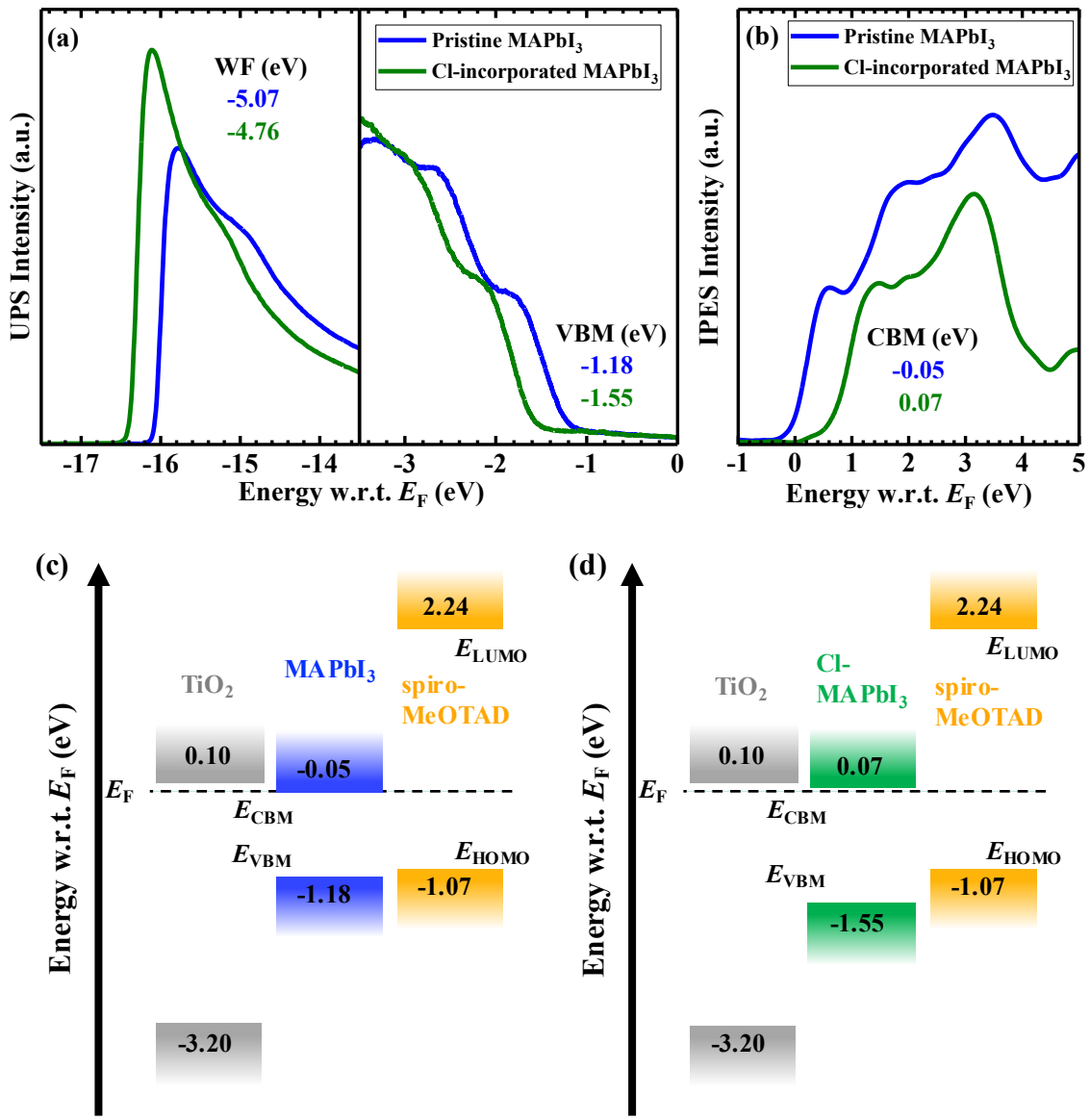

Fig S9: (a) Ultraviolet photoemission spectroscopy (UPS) spectra corresponding to the secondary electron onset region and valence features and (b) inverse photo emission spectroscopy (IPES) measurement results acquired on the pristine $MAPbI_3$, film (thickness ~ 4-5 nm) and $PbCl_2$ (0.75 ML) deposited $MAPbI_3$ perovskite film (thickness ~ 4-5 nm) deposited on Au(111). (c-d) Energy diagrams with respect to (w.r.t.) the Fermi level (E_F) for the pristine $MAPbI_3$ and $PbCl_2$ deposited $MAPbI_3$ film sandwiched between spiro-MeOTAD HTL[2] and TiO_2 ETL[1] as an example of a solar cell architecture.

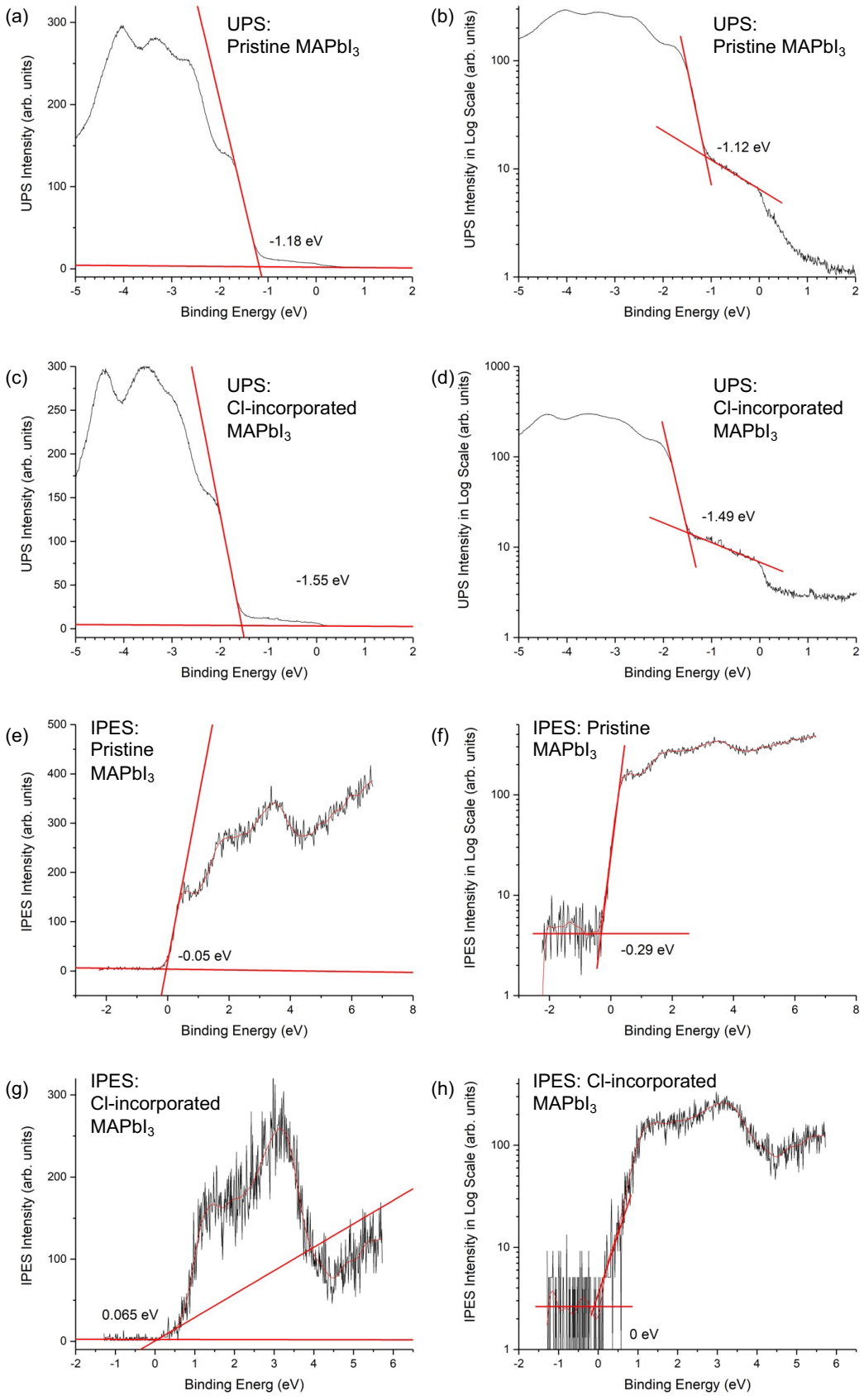

Fig S10: (a-d) UPS and (e-h) IPES spectra of the pristine $MAPbI_3$ and Cl-incorporated $MAPbI_3$ and the VBM and CBM determination considering the intensity in (a,c,e,g) linear and (b,d,f,h) logarithmic scales.

References:

1. Schulz, P.; Edri, E.; Kirmayer, S.; Hodes, G.; Cahen, D.; Kahn, A., Interface energetics in organo-metal halide perovskite-based photovoltaic cells. *Energy Environ. Sci.* **2014**, *7*, 1377-1381.

2. Hawash, Z.; Ono, L. K.; Raga, S. R.; Lee, M. V.; Qi, Y. B., Air-Exposure Induced Dopant Redistribution and Energy Level Shifts in Spin-Coated Spiro-MeOTAD Films. *Chem. Mater.* **2015**, *27*, 562-569.

3. Wang, Y.; Dar, M. I.; Ono, L. K.; Zhang, T.; Kan, M.; Li, Y.; Zhang, L.; Wang, X.; Yang, Y.; Gao, X.; Qi, Y. B.; Grätzel, M.; Zhao, Y., Thermodynamically stabilized β-$CsPbI_3$–based perovskite solar cells with efficiencies >18%. *Science* **2019**, *365*, 591-595.

5. Hu, Z.; Lin, Z.; Su, J.; Zhang, J.; Chang, J.; Hao, Y., A Review on Energy Band-Gap Engineering for Perovskite Photovoltaics. *Solar RRL* **2019,** *3*, 1900304.

6. Xu, J.; Boyd, C. C.; Yu, Z. J.; Palmstrom, A. F.; Witter, D. J.; Larson, B. W.; France, R. M.; Werner, J.; Harvey, S. P.; Wolf, E. J.; Weigand, W.; Manzoor, S.; van Hest, M. F. A. M.; Berry, J. J.; Luther, J. M.; Holman, Z. C.; McGehee, M. D., Triple-halide wide–band gap perovskites with suppressed phase segregation for efficient tandems. *Science* **2020,** 367, 1097-1104.